JOURNAL OF SOLID STATE CHEMISTRY 27, 55–70 (1979)

The Application of Electron Microscopy and Electron Diffraction to Solid State Chemistry Problems*

G. VAN TENDELOO, D. VAN DYCK, J. VAN LANDUYT, AND S. AMELINCKX†

Rijksuniversitair Centrum Antwerpen, Groenenborgerlaan 171, B-2020 Antwerp, Belgium.

Received May 30, 1978

The application of high-resolution electron microscopy and selected area electron diffraction to problems of solid state chemistry is illustrated by means of a number of case studies. Various stackings in mixed-layer compounds such as barium ferrites and lanthanum–thorium mixed oxides and in polytypic substances such as YSeF can be revealed by means of lattice and structure images. Detailed information on the domain structure of alloys such as Au_5Mn_2 and Au_4Mn can be obtained by the use of structure images which reveal columns of single atoms (in Au_4Mn) and (or) pairs of atoms (in Au_5Mn_2). Along inclined twin interfaces high-resolution electron microscopy allows the coincidence lattice on an atomic level to be revealed.

1. Introduction

In recent years high-resolution electron microscopy and electron diffraction have become powerful tools complementing X-ray diffraction in the determination of crystal structures and in particular in the study of deviations from stoichiometry of such structures. Where X-ray diffraction becomes difficult to apply as the unit cell size gets larger, electron microscopy becomes the more adequate tool. It allows one to visualize directly the stacking sequences in polytypes and mixed-layer compounds, even if only "lattice" images can be produced. In such cases an image code based on known sequences can be deduced and applied to unknown sequences (*1, 2*).

In favorable circumstances it is possible to produce "structure" images also. In particular this can be done for "column" structures, i.e., structures in which columns parallel to the viewing direction contain only atoms of the same chemical species. In such structures the imaging conditions can be chosen such that the images are rather independent of focus and foil thickness, and hence can be interpreted in terms of columns of atoms. It is possible to study in such crystals deviations from strict periodicity on an atomic level (*3, 4*).

It is the purpose of this paper to illustrate the use of lattice and structure images in the study of a few different classes of crystals.

2. Lattice Imaging of Mixed-Layer Compounds and Polytypes

2.1. Barium ferrites (*1*)

The structure of the barium ferrite is based on the close-packed stacking of oxygen ions.

* Based on an invited lecture presented by S. Amelinckx. Work performed under the auspices of the association RUCA–SCK.

† Also at SCK–CEN, B-2400 Mol (Belgium).

0022–4596/79/010055–16$02.00/0

The two basic stackings are shown in Fig. 1, where the lowercase letter represents close-packed oxygen layers and the capital letters mixed barium oxygen layers the structure of which is represented in Fig. 1a.

The hexagonal M structure (Fig. 1b) has the composition $BaFe_{12}O_{19}$; it contains two blocks with a thickness of 11.6 Å per unit cell. The blocks M_1 and M_2 are rotated with respect to each other by an angle of 180° about the c-axis. The barium-containing layer is in fact a mirror plane for the structure. The subdivision into blocks is of course arbitrary; however, the choice made here emphasizes the symmetry within a single block and shows that only two positions are used in each block, for the oxygen layers.

The rhombohedral Y structure has the composition $Ba_2Me^{II}Fe_{12}O_{22}$ (Me^{II} = Zn). It contains three blocks with a thickness of 14.52 Å per unit cell. The choice of blocks made here, again emphasizes the fact that in each block only two positions are used for the oxygen layer.

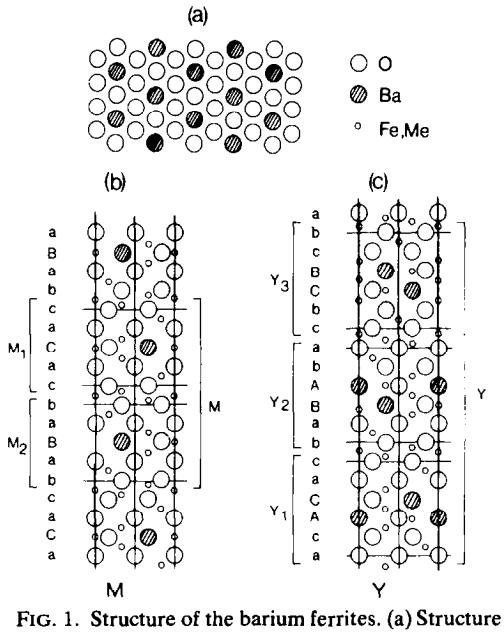

FIG. 1. Structure of the barium ferrites. (a) Structure of the close packed O and BaO layers. (b) Structure of the pure M compound. (c) Structure of the pure Y compound.

In both structures the contact between blocks, as defined above, is realized by means of two triplet layers in the cubic arrangement. This seems to be a general building principle which is obeyed in all known mixed-layer compounds of the type M_nY_m.

The central row dark field lattice images for a number of mixed-layer compounds of the series M_nY_m are reproduced in Fig. 2. The most striking feature is the occurrence of dark lines with two different spacings closely corresponding to 11.6 and 14.5 Å. It is therefore very tempting to associate the pairs of more closely spaced lines with an M block and the pair of more widely spaced lines with a Y block. This very simple imaging code allows one to explain consistently the structures of those compounds for which the structure was known from X-ray diffraction. It therefore seems justifiable to extend this interpretation to compounds the structure of which had not been previously determined. Table I summarizes the interpretation of the line sequences of Fig. 2. Note that in all these sequences the M blocks appear isolated, whereas the Y blocks form bands.

With noncentral row dark field images used, successive Y bands separated by an M block exhibit different shades, showing that these mixed-layer compounds are in fact polysynthetic twins (Fig. 3) and allowing an easy interpretation of these structures in terms of subunit cell level twinning.

In the present case the polysynthetic twinning can be considered as a means of accommodating different O : Ba ratios in the structure. A schematic representation of the twinned structure is given in Fig. 4.

2.2. Lanthanum–Thorium Mixed Oxides *(5)*

In the system of mixed oxides La_2O_3–ThO_2, a number of well-defined compounds have been identified by Sibieude and Foex (*6, 7*). The structures of these compounds, as determined by means of X-ray diffraction, as well as the structure of the pure end members of the series, are represented in Fig. 5.

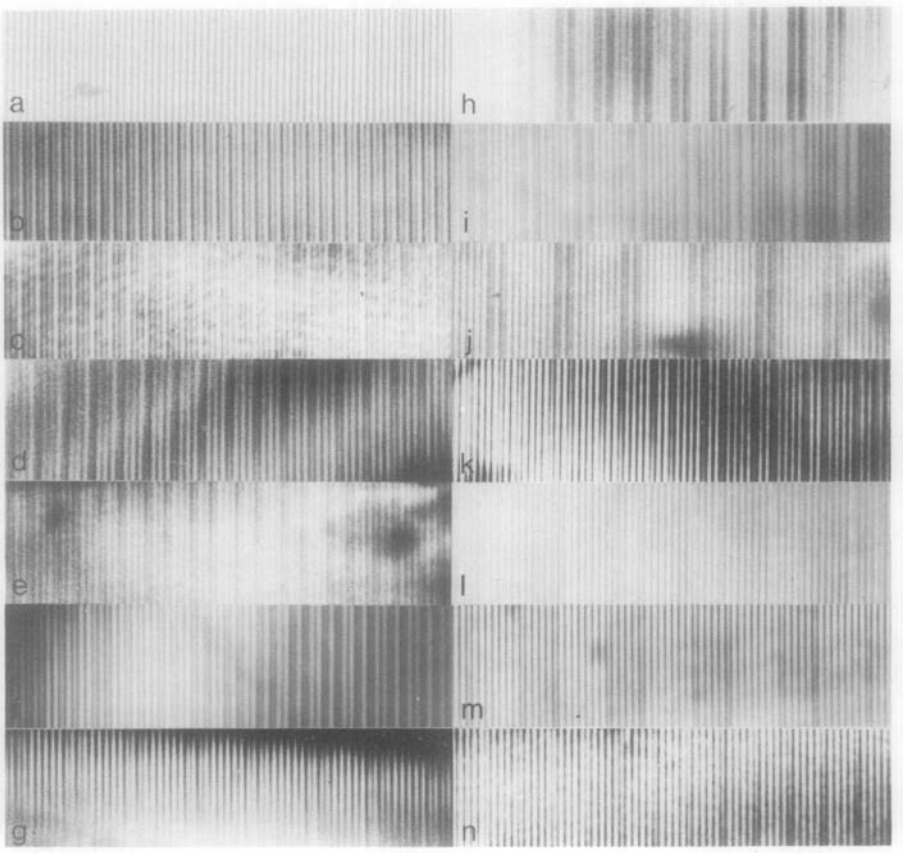

FIG. 2. Lattice images for a number of different compounds of type M_nY_m. The corresponding stacking sequences are given in Table I.

TABLE I

$M:Y$	Stacking sequence	Figure
1:∞	Y	2a
2:1	MMY	2c
2:2	$MYMY$	2b
2:3	$MYMY_2$	2f
2:4	$MYMY_3$	2h
2:5	MY_2MY_3	2e
2:6	$MYMY_5$	2i
	MY_2MY_4	2k
	MY_3MY_3	2d
2:7	$MYMY_6$	2g
2:8	$MYMY_7$	2j
	MY_4MY_4	2n
2:10	MY_3MY_7	2l
2:11	MY_4MY_7	2m

The ψ compounds were studied by Sibieude and Foex (*6*) and from their results the general building principle of these compounds can be deduced. The stacking of the oxygens, represented by capital letters in Fig. 5, is cubic close packed. The lanthanum atoms, represented by lowercase letters, as well as the thorium atoms, represented by greek letters, occupy octahedral interstices in this oxygen arrangement. ThO_2, which has the fluoride structure, can then be represented by the stacking symbol

$$C|\alpha BA\ \beta CB\ \gamma AC|\alpha \quad \text{or} \quad T_1T_2T_2\cdots$$
$$T_1\quad T_2\quad T_2$$

whereas the stacking symbol of the structure

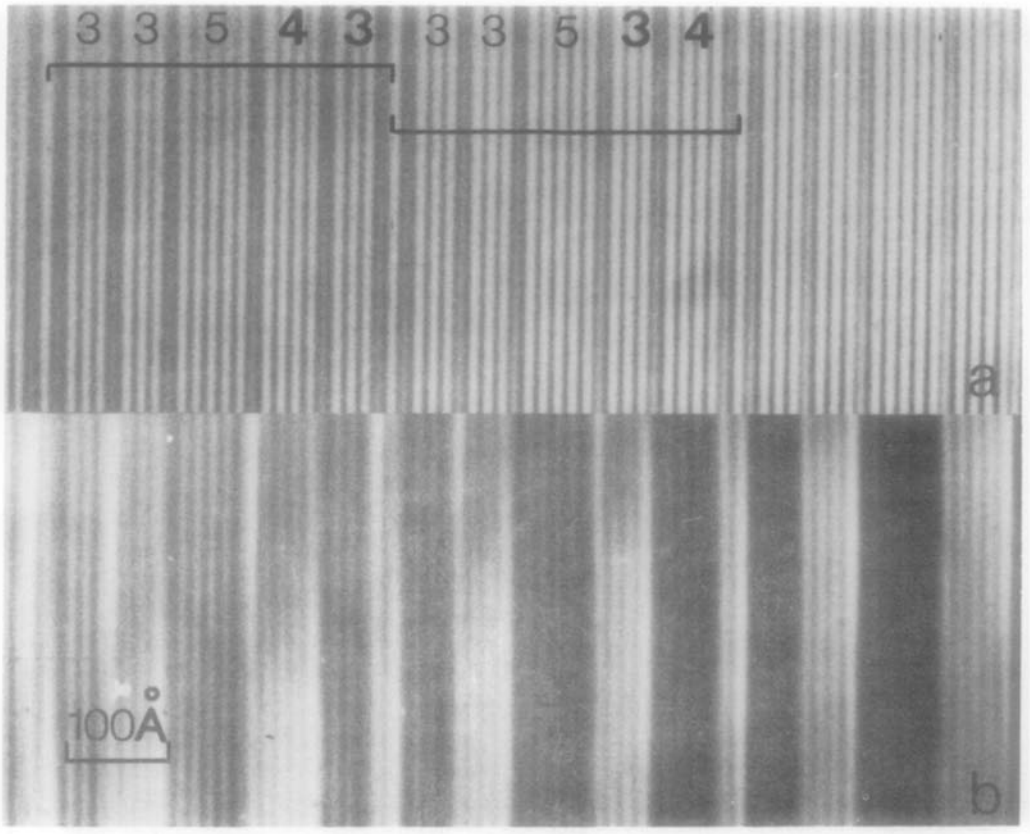

FIG. 3. Noncentral row dark field image. Note the correspondence between band image and line image. The part shown contains a sequential fault.

of La_2O_3 can be written as

$$a\,B|A\,b\,C\,a\,B|A\,b\ldots \quad \text{or} \quad L\ldots.$$

The mixed oxides are composed of regular alternations of L and T blocks and can thus be represented by symbols such as

$$TL \quad (9R \quad \text{or} \quad \psi_3),$$
$$TTL \quad (12R \quad \text{or} \quad \psi_4),$$
$$TLL \quad (15R \quad \text{or} \quad \psi_2).$$

From the c parameter of the unit cells of these compounds one can deduce the average thicknesses of an L and a T block. One finds ~6.1 Å for an L block and ~3.3 Å for a T block.

Preliminary results of a systematic study of specimens with different compositions have revealed a great analogy with the barium ferrites. Lattice images reveal lines with different spacings which can again be assimilated with L and T blocks (*5*). Two-dimensional images could be produced in this case. Figure 6a shows a known sequence $12R(\psi_4)$,

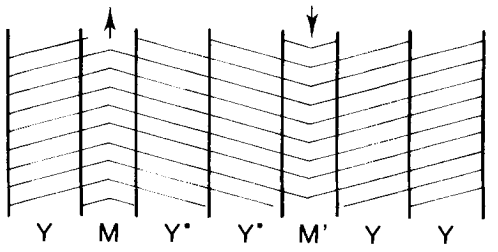

FIG. 4. Model of polysynthetic twins. The twin plane is associated with the M blocks; Y^* is the twinned version of Y.

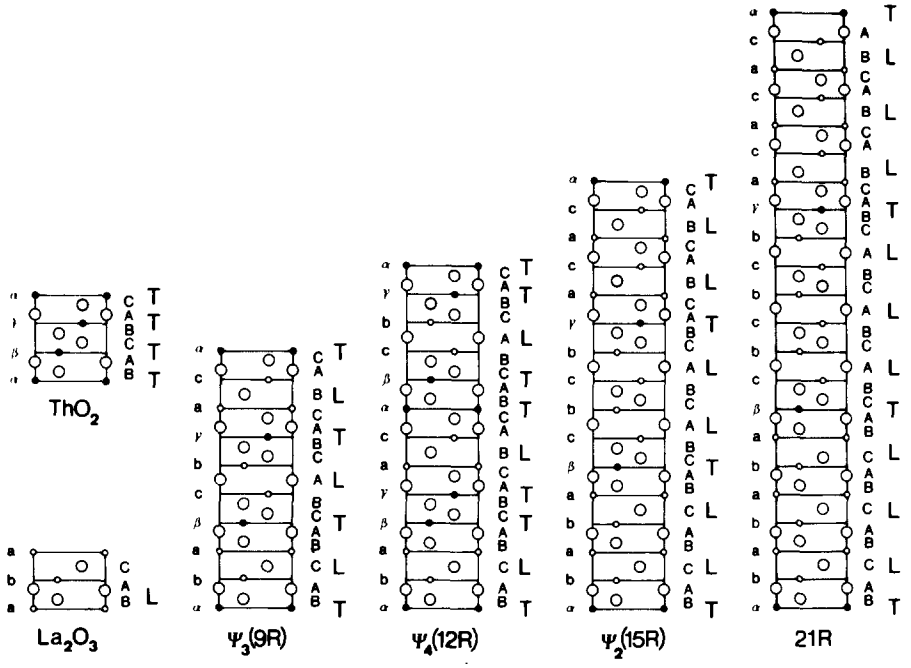

FIG. 5. Structures of mixed oxides in the system La_2O_3-ThO_2. *L* represents an La_2O_3 block and *T* a ThO_2 block (after Sibieude).

together with a correctly scaled representation of the structure, whereas Fig. 6b shows a newly discovered sequence $21R$ and the corresponding structure.

2.3. YSeF-Polytypes

In this compound Dagron *et al.* (*8*) have found different polytypes by means of X-ray diffraction. These polytypes were found to be built up by the periodic stacking of two types of unit blocks, hereafter called *S* and *T*. These blocks have the same *a* and *b* parameters, but the enclosed angles are each other's supplements. The different polytypes belong to two different series:

(1) The monoclinic series, designated by the symbol *M*. The lattice constants obey the simple relation

$$b = nb_0/\sin\gamma, \qquad b_0 = 3.15\ \text{Å},$$
$$b\cos\gamma = a_3.$$

Monoclinic polytypes with *n* values equal to 2, 4, 6, 8, 10 and 12 were identified.

(2) The orthorhombic series, designated by the symbol O. It obeys the relation $b = nb_0$ with $n = 2$, 6, and 14.

The structures of the compounds 2O, 6O, and $4M$ were determined by means of X-ray diffraction (*8*) and could therefore be used to derive an image code. These structures are shown in Figs. 7a–c, whereas the corresponding images are shown in Figs. 8a–c. These structures can be described in terms of *S* and *T* blocks by means of the symbols

$$6O: \ldots |SSSTTT|SSSTTT|,$$
$$2O: \ldots |STST|,$$
$$4O: \ldots |SSST|SSST| \ldots .$$

From the images it is clear that the zig-zag lines give information on the succession of *S* and *T* blocks directly. Using this imaging code we could deduce the stacking sequences of compounds such as $6M$, $8M$, $10M$, $12M$, and $14M$, as well as 14O. Subsequent X-ray diffraction studies of some of these

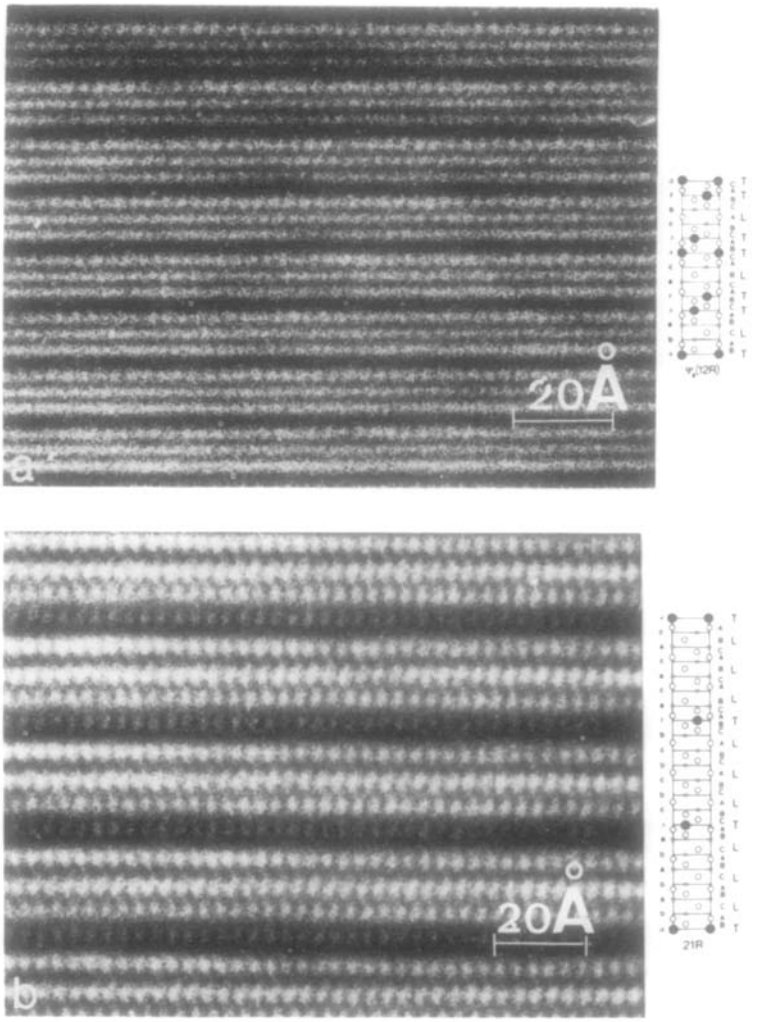

FIG. 6. Structure images of mixed lanthanum–thorium oxides. (a) ψ_4 (12R); (b) 21R.

compounds have confirmed the structures as deduced from the images (*9*).

Figures 9a and b shows the images and the structures, as deduced from the images, for two of these compounds: 8M and 12M.

3. Structure Imaging in Ordered Alloys

3.1. Structures

A number of alloy phases in the system Au–Mn have structures which can be described as consisting of parallel columns containing only atoms of a given chemical species. The structures of Au_5Mn_2 (*3*) and Au_4Mn (*4*) are two simple examples; these structures are represented in Fig. 10, where small circles represent gold and large circles manganese, both at two different levels: 0 or $\frac{1}{2}$. We call structures which have these features "column structures."

Both structures are superstructures of the basic fcc structure; the diffraction pattern thus consists of spots which reveal the superstructure. In the particular cases considered

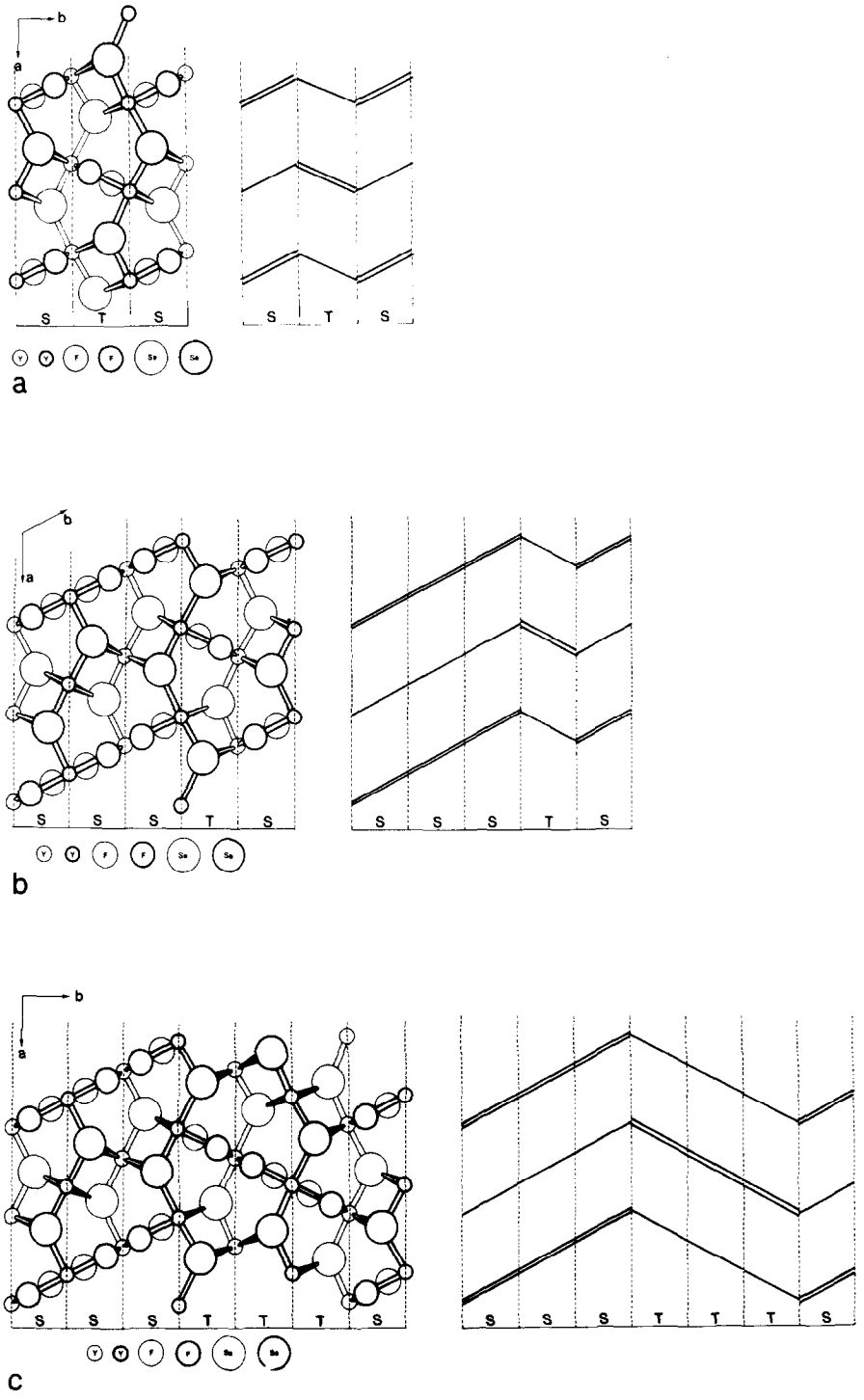

FIG. 7. Structures of the polytypes of YSeF (after ref. (*8*)); atomic representation as well as schematic representation. (a) 2O; (b) 6O; (c) 4*M*.

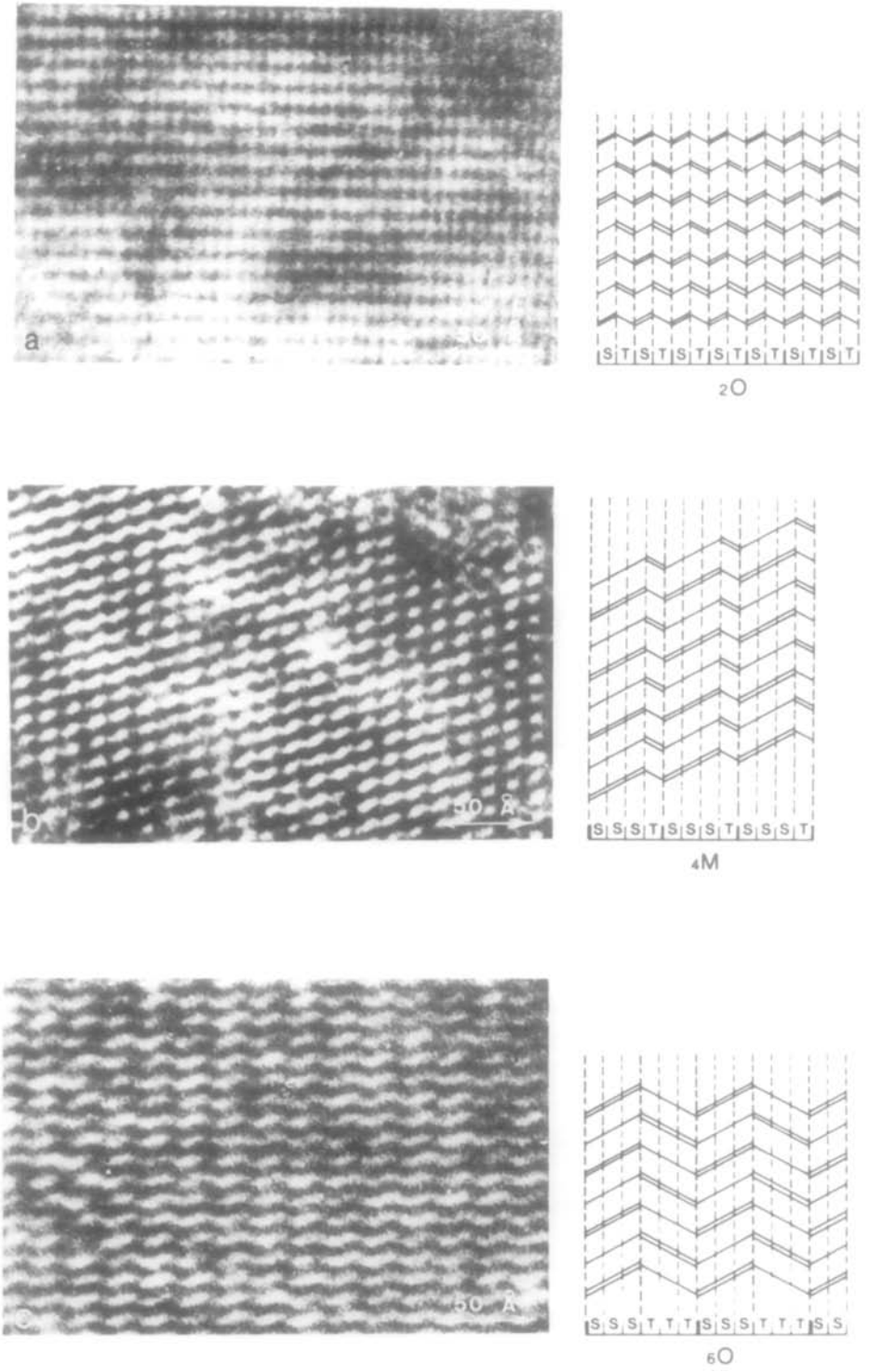

FIG. 8. Structure images of different polytypes of YSeF used to derive the image code (a) 2O; (b) 4*M*; (c) 6O.

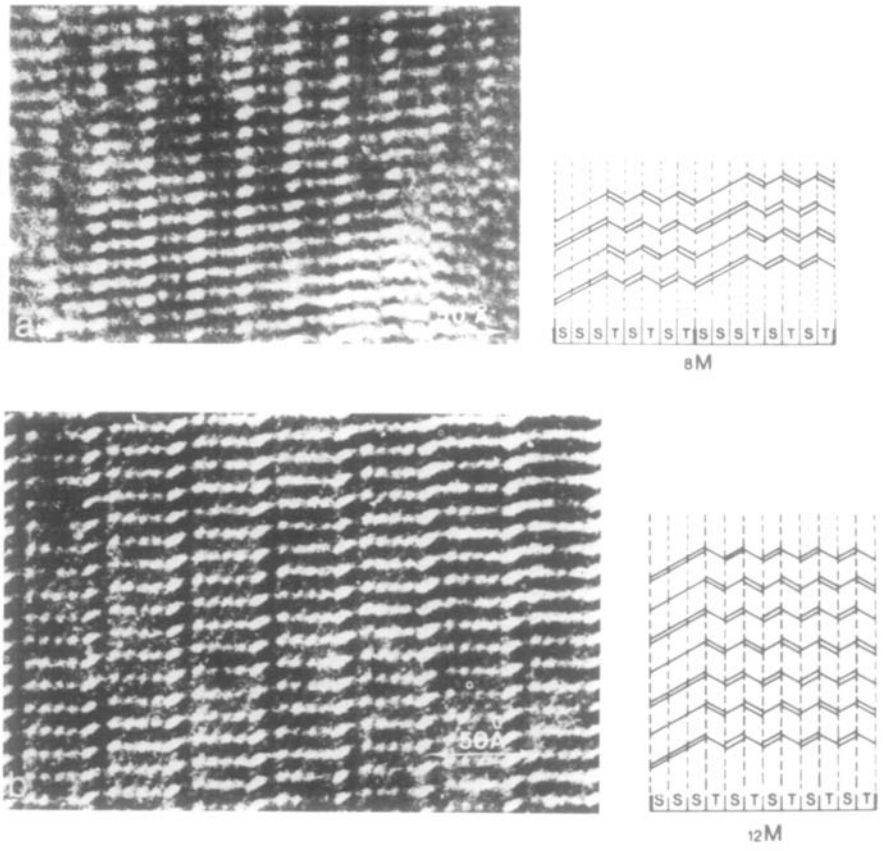

FIG. 9. Structure images of polytypes the structure of which was deduced by means of electron microscopy. (a) $8M$; (b) $12M$.

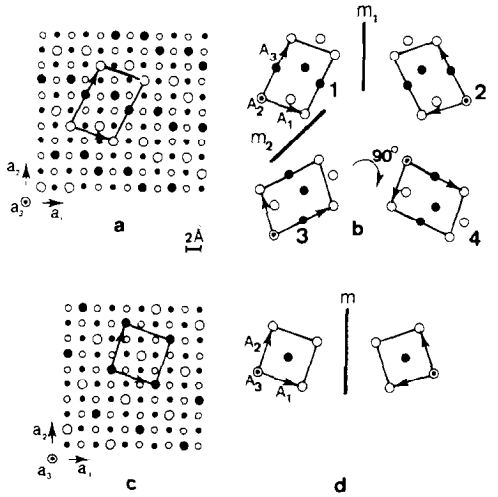

FIG. 10. Structures of Au_5Mn_2 and Au_4Mn and coaxial structural variants. (a) Au_5Mn_2; (b) Four coaxial structural variants of Au_5Mn_2; (c) Au_4Mn; (d) Two coaxial variants of Au_4Mn.

the superstructure spots reveal the arrangement of the minority atoms, i.e., the manganese atoms. To make structure images one can now orient the crystal with the electron beam parallel to the direction of the columns and collect in the selector aperture only superstructure spots excluding the basic spots. In such a way redundant information is rejected and only the most relevant part of the information is collected.

The images of Fig. 11 have been produced in this manner; they can be compared directly with the structures of Figs. 10a and 10c. It is then easy to see that the columns of the structures are imaged as bright dots (or as dark dots in Fig. 11c).

In the case of Au_4Mn the configuration of bright dots is exactly the same in size and orientation as that of columns of single

manganese atoms when the structure is viewed along the cube direction parallel to the columns (compare Figs. 10c and 11b).

Also in Au_5Mn_2 the configuration of elongated bright dots is exactly the same in size and orientation as the configuration of columns of close pairs of manganese atoms when the structure is viewed along the cube direction parallel to the columns of pairs, i.e., along the *b*-axis (compare Figs. 10a and 11a).

These observations strongly suggest that the bright dots (or dark dots under certain conditions) image columns of single atoms in Au_4Mn or of close pairs of manganese atoms in Au_5Mn_2. The image is not strongly dependent on focus or foil thickness. Image calculations using multiple beam dynamical theory have confirmed this interpretation in the case of Au_5Mn_2; they also confirm the relative independence of the image on focus and on foil thickness. There is little doubt that this interpretation also applies to Au_4Mn. Below we present evidence supporting our interpretation of images in terms of columns of atoms.

3.2. Domain Structures

Since one can "see" the structure in the alloys Au_5Mn_2 and Au_4Mn it is a straightforward matter to study their domain structures. We shall give a short survey of such a study; for more detail we refer to the original papers (*3, 10*).

3.2.1. Au_4Mn

As shown above, the alloy Au_4Mn has a tetragonal superstructure of the fcc structure. This tetragonal structure can be formed in six different orientation variants with respect to the fcc basic structure (Fig. 12) (*11*). Along any one of the three cube directions two coaxial variants are possible. The atom columns in both parts of the coaxial twin (also called "anti-parallel twin" in Ref. (*11*)) are parallel with a common cube direction. They can thus be imaged simultaneously. Figure 13 shows such an image. The presence of two orientation variants in the same configuration as that in Fig. 12 is obvious.

The image also reveals the antiphase boundaries (APB) as sideways offsets of rows of atom columns. The orientation of the APBs is highly preferential; they often form angular arrangements, with the two parts mutually perpendicular. The APB energy is clearly very anisotropic.

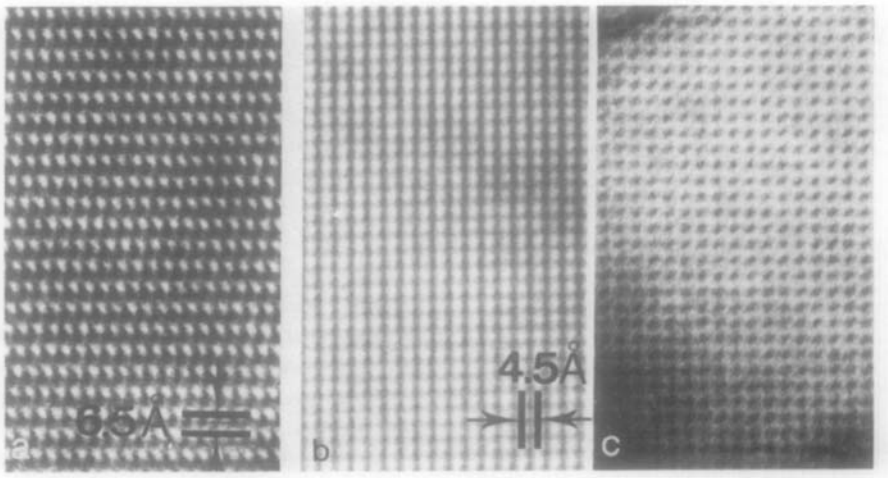

FIG. 11. Structure images of Au_4Mn and Au_5Mn_2. (a) Au_5Mn_2. (b) Au_4Mn (bright dots). (c) Au_4Mn (dark dots).

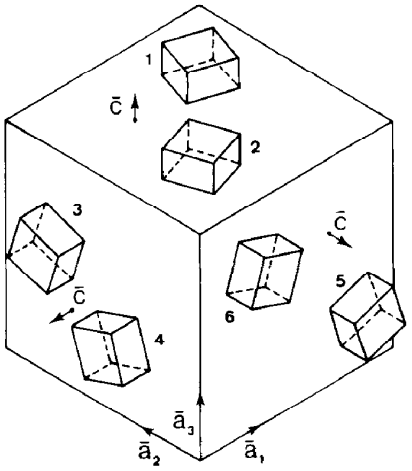

FIG. 12. The six orientation variants of Au_4Mn.

3.2.2. Au_5Mn_2

The alloy Au_5Mn_2 has a monoclinic superstructure of the fcc structure. It can be built in 12 different orientation variants with respect to the fcc basic structure (*10*). These 12 orientation variants are represented schematically with respect to the basic cube in Fig. 14. Along any cube direction four coaxial variants with a common column direction along the *b*-axis are present. The structures of these four variants can thus be imaged simultaneously. In this way three different coaxial twin interfaces can be revealed directly (Fig. 15).

In Fig. 16 images of such interfaces are reproduced.

1° (100) reflection twins (Fig. 16a),

2° (110) reflection twins (Fig. 16b),

3° 90° rotation twins (Fig. 16c).

The "atomic" structure in the interface can be studied in detail assuming that the white dots represent columns of manganese pairs (*12*).

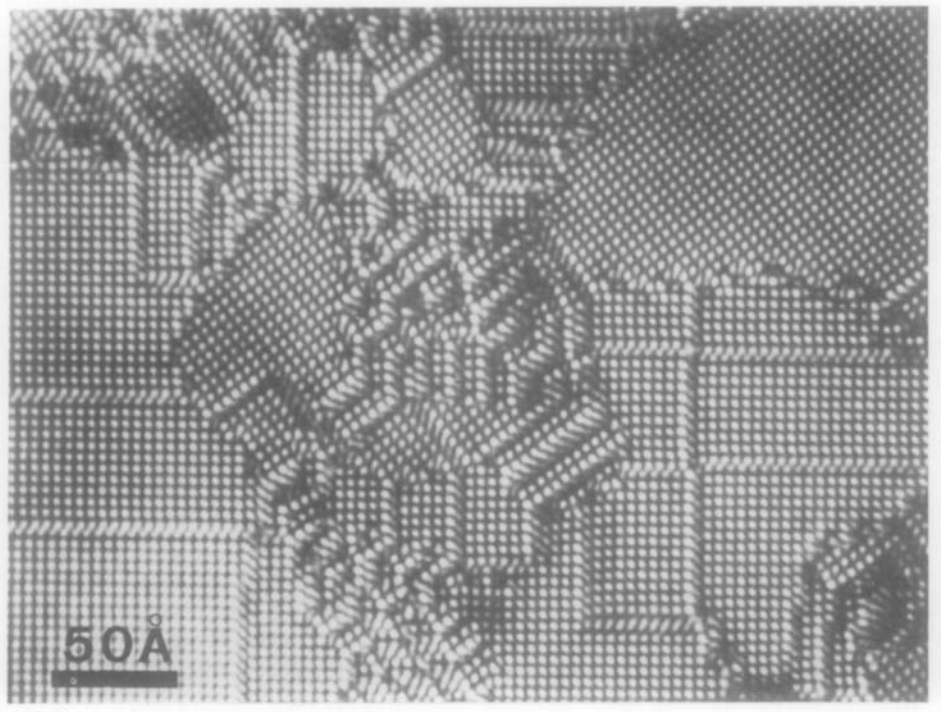

FIG. 13. Structure image of Au_4Mn showing domain structure; note the presence of two coaxial variants and of numerous APBs.

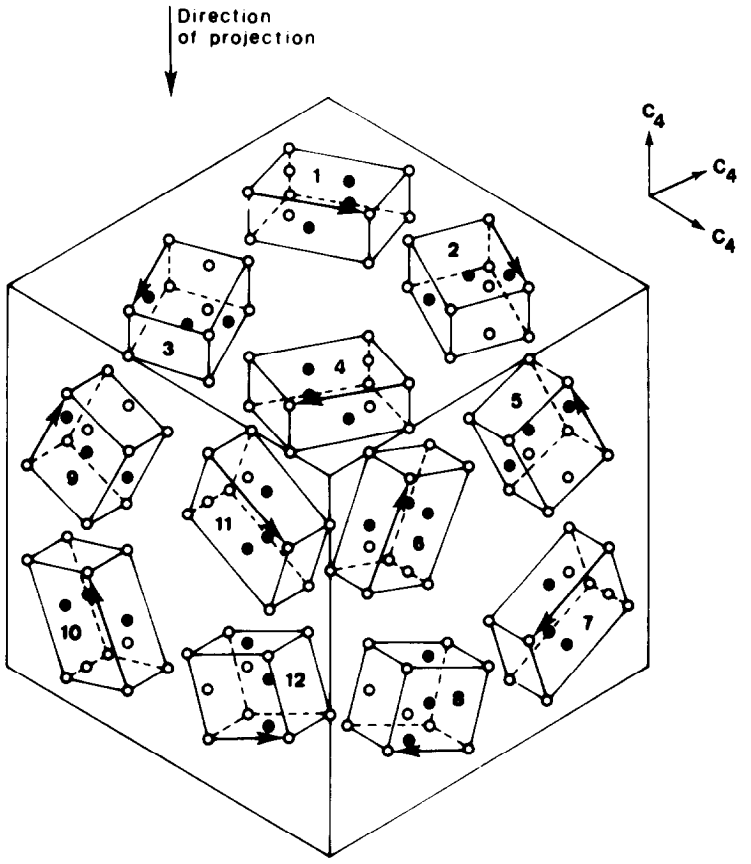

FIG. 14. The 12 orientation variants of Au_5Mn_2.

3.3 Coincidence Structure, Coincidence Lattice (*12*)

3.3.1. Twins in Au_4Mn

When the interfaces between coaxial variants in Au_4Mn are inclined with respect to the column direction, dot patterns result in the overlap part, as shown in Fig. 17. The interpretation of these dots in terms of atom columns is straightforward.

Let us assume that the atom columns in both parts of the coaxial twin continue undisturbed up to the interface. In Fig. 18 we represent columns in one part as full dots and columns in the twinned part as open dots. The coincidence pattern, i.e., the pattern of columns which are continuous across the interface, is then a square grid with an edge equal to $2.5a$ (a = lattice parameter of fcc basic structure). The geometry of this overlap pattern is exactly the same in orientation and in size as that of the bright dots in Fig. 17. It is thus clear, beyond any reasonable doubt, that the pattern of bright dots reveals the coincidence pattern on an atomic level. This simple geometrical model for a coincidence pattern is thus quite adequate.

The model proves at the same time that continuous columns are revealed as extra white dots and supports our interpretation of the image of column structures. Contrast is best close to the center of the overlap region. Near the edges of the overlap region a continuous transition from the overlap pattern into the dot pattern characteristic of the adjacent domain is observed. This is

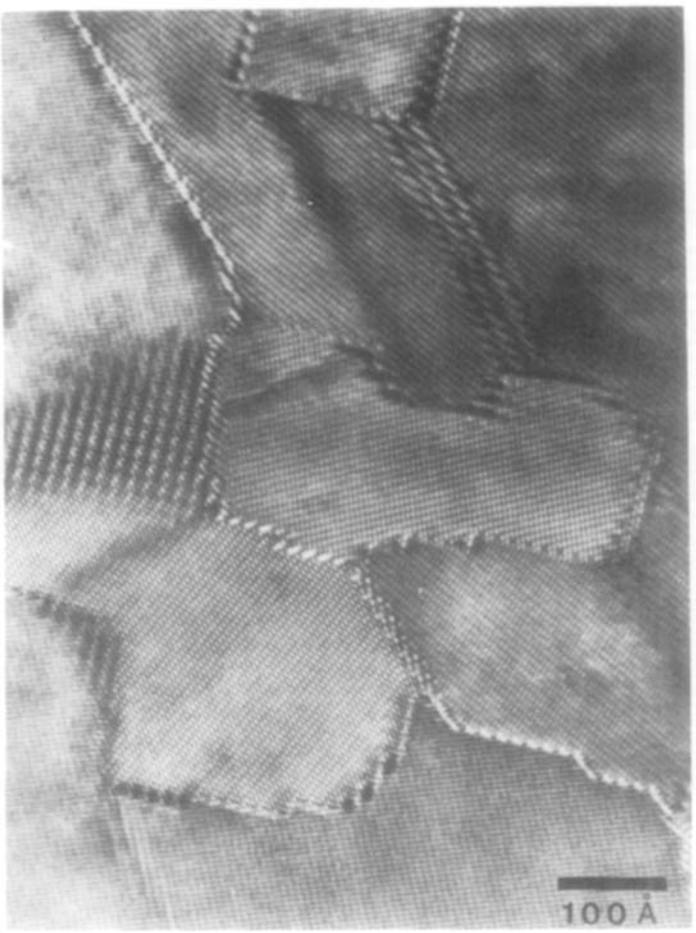

FIG. 15. Structure image of Au_5Mn_2 showing domain structure.

consistent with the simple geometrical model. It is clear from Fig. 19 that close to the center of the overlap regions the coincidence columns are most markedly differentiated from the noncoincidence columns. Close to the edges this difference gradually disappears.

3.3.2. Effect of the Presence of an Antiphase Boundary

It is of some interest to consider the effect on the coincidence pattern of a parallel translation of one of the domains. This effect can be revealed directly in an overlap region intersected by an antiphase boundary; a spatial view of such a situation is shown in Fig. 20.

Similar coincidence patterns are observed at overlapping parts of domain boundaries in Au_5Mn_2. However, in this case the coincidence structure is different for the three types of coaxial domain boundaries; the coincidence lattice is the same; the motif is different.

In the geometrical model of Fig. 21 the manganese columns in one part are represented by full dots, whereas the manganese columns in the second domain, which contains an antiphase boundary with a displacement vector R, are represented by

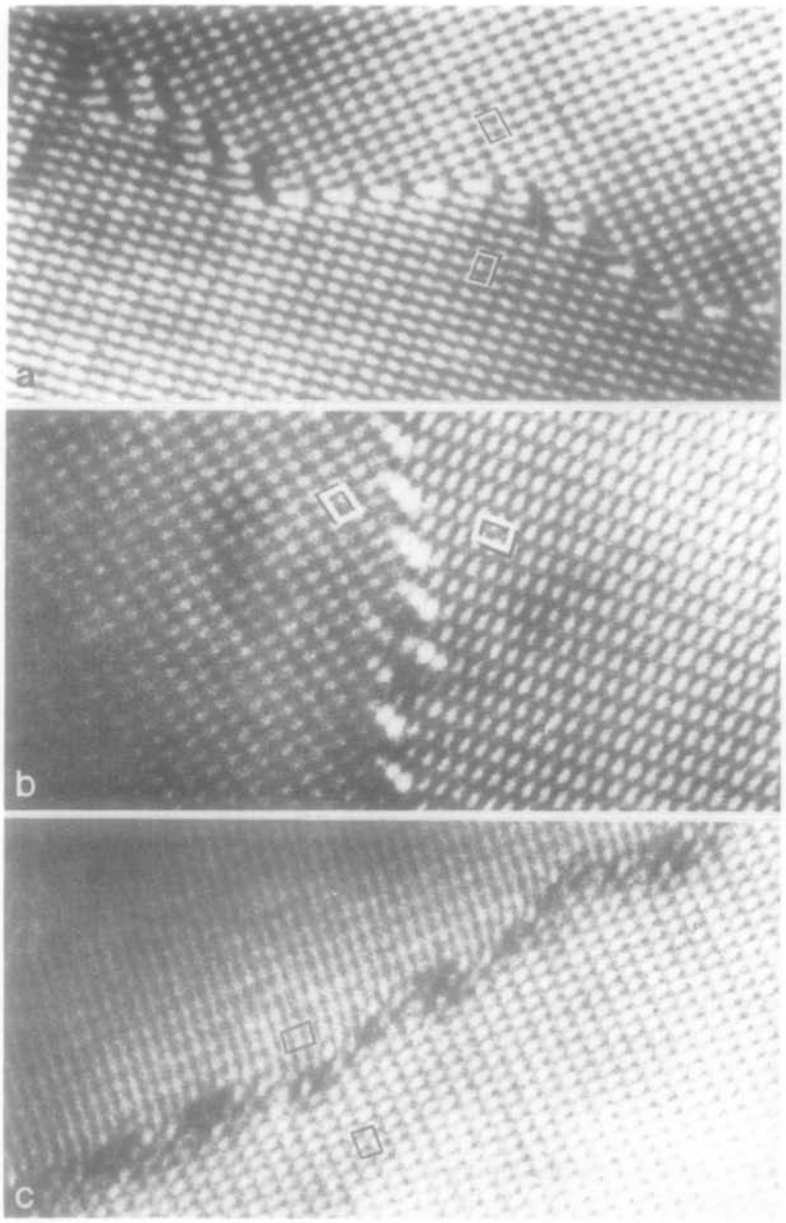

FIG. 16. Different types of interfaces between coaxial variants. (a) (100) mirror twin; (b) (110) mirror twin; (c) 90° rotation twin.

open circles. It is obvious that the coincidence patterns on either side of the antiphase boundary have suffered a relative shift over a vector S which is larger than R.

Such a shift is visible in Fig. 17, where the APB is indicated. The correspondence between the geometrical model and the observed configuration is striking.

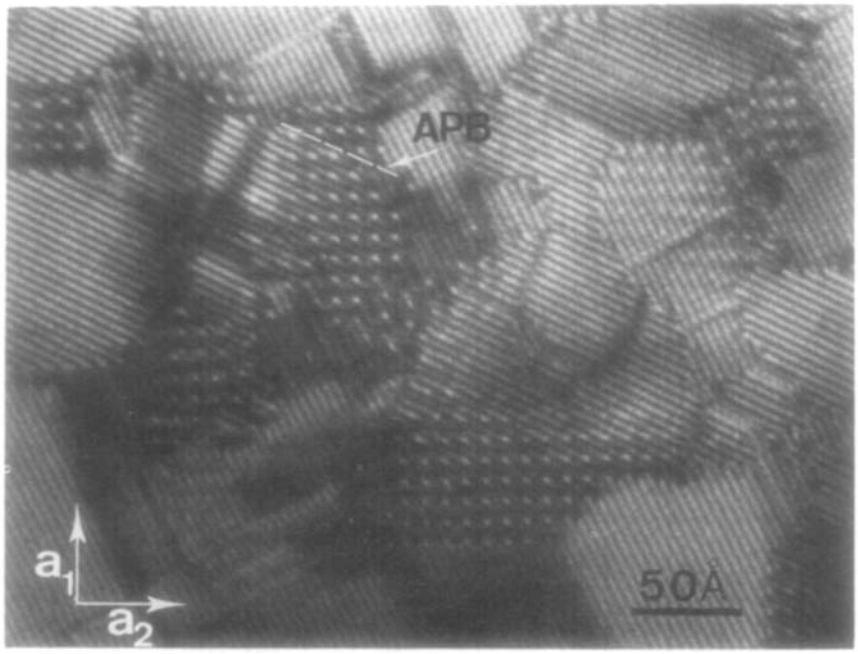

FIG. 17. Coincidence pattern in Au_4Mn. Note the presence of an APB and the associated shift of the coincidence pattern.

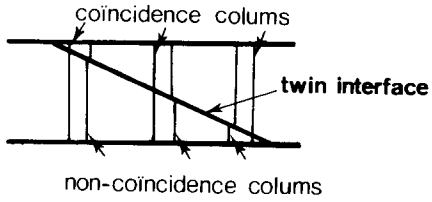

FIG. 19. Schematic representation of coincidence and noncoincidence columns.

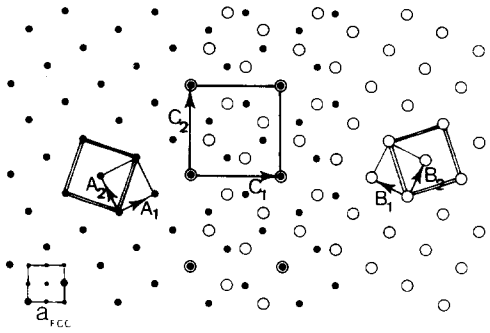

FIG. 18. Geometrical model for the coincidence pattern of coaxial variants in the Au_4Mn structure.

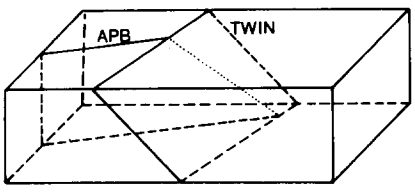

FIG. 20. Intersection of APB with twin domain boundary.

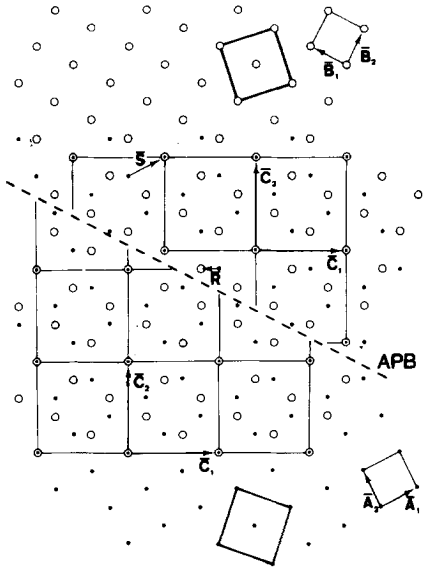

FIG. 21. Shift of coincidence pattern due to the presence of an APB. This model can be compared with Fig. 17.

4. Conclusion

In this paper we have described a few typical examples of the application of high-resolution electron microscopy to structural problems. It is to be expected that in the future solid state chemistry will benefit to an increasing extent from the results of high-resolution electron microscopy.

Acknowledgment

Thanks are due to Dr. F. Casteels (S.C.K. Mol) for the preparation of the mixed oxides of Lanthanum and Thorium.

References

1. J. VAN LANDUYT, S. AMELINCKX, J. A. KOHN, AND D. W. ECKART, *J. Solid State Chem.* **9**, 103 (1974).
2. D. VAN DYCK, J. VAN LANDUYT, S. AMELINCKX, NGUYEN HUY-DUNG, AND C. DAGRON, *J. Solid State Chem.* **19**, 179 (1976).
3. G. VAN TENDELOO, R. WOLF, D. VAN DYCK, AND S. AMELINCKX, *Phys. Status Solidi.*, **47**, 105 (1978).
4. G. VAN TENDELOO AND S. AMELINCKX, *Phys. Status Solidi.*, **49**, 337 (1978).
5. D. VAN DYCK *et al.*, *J. Solid State Chem.* in preparation.
6. F. SIBIEUDE AND M. FOEX, *J. Nucl. Mater.* **56**, 229 (1975); F. SIBIEUDE, *C.R. Acad. Sci. Paris, Ser. C* **271**, 130 (1970).
7. F. SIBIEUDE, *J. Solid State Chem.* **7**, 7 (1973).
8. C. DAGRON, *Compt. Rend. Ser. C* **275**, 817 (1972); N. HUY-DUNG, *Acta Crystallogr. B* **29**, 2095 (1973); N. HUY-DUNG, C. DAGRON, AND P. LARUELLE, *Acta Crystallogr. B* **31**, 514, 519 (1975).
9. This conference.
10. G. VAN TENDELOO, R. WOLF, AND S. AMELINCKX, *Phys. Status Solidi A* **40**, 531 (1977).
11. E. RUEDL, P. DELAVIGNETTE, AND S. AMELINCKX, *Phys. Status Solidi* **28**, 305 (1968).
12. G. VAN TENDELOO AND S. AMELINCKX, *Phys. Status Solidi*, **47**, 555 (1978).